

Machine Learning of Explicit Order Parameters: From the Ising Model to SU(2) Lattice Gauge Theory

Sebastian J. Wetzel¹ and Manuel Scherzer¹

¹*Institut für Theoretische Physik, Universität Heidelberg, Philosophenweg 16, 69120 Heidelberg, Germany*

We present a procedure for reconstructing the decision function of an artificial neural network as a simple function of the input, provided the decision function is sufficiently symmetric. In this case one can easily deduce the quantity by which the neural network classifies the input. The procedure is embedded into a pipeline of machine learning algorithms able to detect the existence of different phases of matter, to determine the position of phase transitions and to find explicit expressions of the physical quantities by which the algorithm distinguishes between phases. We assume no prior knowledge about the Hamiltonian or the order parameters except Monte Carlo-sampled configurations. The method is applied to the Ising Model and SU(2) lattice gauge theory. In both systems we deduce the explicit expressions of the known order parameters from the decision functions of the neural networks.

I. INTRODUCTION

Machine learning enables computers to learn from experience and generalize their gained knowledge to previously unseen problems. The development of better hardware and algorithms, most notably artificial neural networks, propelled machine learning to one of the most transformative disciplines of this century. Nowadays such algorithms are used to classify images [1], to recognize language [2] or to beat humans in complex games [3]. Recently, machine learning has even been successfully employed to tackle highly complex problems in physics [4–15]. It is now possible to classify phases of matter in the context of supervised learning [16–21] only from Monte Carlo samples. Phases can also be found without any information about their existence by unsupervised learning [22–25]. It is a difficult task to interpret what machine learning algorithms learn to classify phases, although a first progress was made using support vector machines [26]. The problem is not inherent to physics, since machine learning algorithms, especially artificial neural networks, exploded in complexity and application, and thus the difficulty of interpreting their decisions increased rapidly. There is still no comprehensive theoretical understanding of what is learned by them [27–30].

In the context of physical phase transitions, we open the neural network black-box, and show that the learned decision functions originate from physical quantities. Not only can we interpret these physical quantities, we can explicitly deduce them without prior knowledge.

To this end we propose a new type of neural network, called correlation probing neural network. It can reduce the complexity of the decision function if it is sufficiently symmetric. Physical quantities are typically highly symmetric. Therefore, this network is ideal for probing whether a physical quantity is responsible for the learned decision function. After reducing the complexity with the correlation probing network, we show that it is possible to fully reconstruct the explicit mathematical expression of the decision function. From this expression

one can then easily extract the quantities by which the neural network distinguishes between phases. This procedure is introduced at the Ising Model, where we find that the neural network predicts the phase by the magnetization and the expected energy per spin. We then demonstrate the power of our method at SU(2) lattice gauge theory, which is a QCD-like theory showing confinement. In this case we find that the decision function is based on a non-local and non-linear order parameter, the so-called Polyakov loop.

Our method might find application where phase transitions are inaccessible by other tools. Since machine learning methods can detect phase transitions in regions of phase diagrams that show a sign problem [17], a possible application in QCD could be the examination of the chiral phase transition or the color-superconducting phase [31–33]. Our method could be employed to study the pseudogap in the two dimensional Hubbard model [34–37]. Another application could be the examination of multicritical points, for which the Hubbard model provides a prominent example in the regime of competing d-wave and antiferromagnetic order [38–41].

II. MODELS

A. Ising Model

The Ising model was originally formulated as a model for interactions between magnetic dipole moments of atomic spins. It is a simple, well studied and exactly solvable model from statistical physics. Those properties make it an ideal testing ground for the application of machine learning methods to physical systems. Its Hamiltonian is

$$H(S) = -J \sum_{\langle i,j \rangle_{nn}} s_i s_j + h \sum_i s_i . \quad (1)$$

In the following, we examine the ferromagnetic Ising model $J = 1$ on the square lattice with vanishing external magnetic field $h = 0$. $\langle i, j \rangle_{nn}$ means summing over nearest neighbors, and $S = (s_1, \dots, s_n)$ denotes a spin

configuration, where $s_i \in \{1, -1\}$. By defining the free energy at a given inverse temperature $\beta = (k_B T)^{-1}$,

$$F(\beta) = -\beta^{-1} \log \left(\sum_i e^{-\beta H(S_i)} \right), \quad (2)$$

thermodynamic quantities such as the expectation value of the energy,

$$\langle E \rangle = -\frac{\partial(\beta F)}{\partial \beta}, \quad (3)$$

can be extracted. By the Ehrenfest classification the Ising model has a second order phase transition, since the specific heat $C_V = \partial \langle E \rangle / \partial \beta$ diverges at $T_c = 2 / (k_B \log(1 + \sqrt{2}))$ [42].

In Landau-Ginzburg theory phases are classified via the order parameter, in the Ising model this is the magnetization

$$\langle M \rangle = \left. \frac{\partial F}{\partial h} \right|_{h=0}, \quad (4)$$

which is zero in the paramagnetic phase and finite in the ferromagnetic phase. Its derivative with respect to the temperature diverges at the critical temperature.

B. SU(2) Lattice Gauge Theory

In this paper we examine SU(2) Yang-Mills theory, which shows confinement, one of the most distinct features of QCD. To this end we employ lattice gauge theory. It was originally proposed by Wilson and Wegner and builds on the idea of discretizing the Euclidean path integral such that the lattice spacing a is a natural cutoff scale. This discretization gives a strong analogy to statistical physics and allows for Monte Carlo simulations of gauge theories. SU(2) gauge theory on the lattice is parametrized by so-called link variables $U_\mu^x \in \text{SU}(2)$. Each lattice point x attaches to one link variable per dimension μ . In this work, we use four-dimensional $N_\tau \times N_s^3$ spacetime lattices with $N_\tau = 2$ (temporal direction) and $N_s = 8$ (spatial volume). The link variables U_μ^x are parametrized by four real parameters,

$$U_\mu^x = a_\mu^x \mathbb{1} + i (b_\mu^x \sigma_1 + c_\mu^x \sigma_2 + d_\mu^x \sigma_3), \quad (5)$$

where σ_i are the the Pauli matrices, the coefficients obey $(a_\mu^x)^2 + (b_\mu^x)^2 + (c_\mu^x)^2 + (d_\mu^x)^2 = 1$. The trace of U_μ^x is given by $2 a_\mu^x$, since the Pauli matrices are traceless. Link variables are objects that live on the links between two neighbouring sites. They transform under gauge transformations via

$$U_\mu^x \rightarrow \Omega^x U_\mu^x (\Omega^{x+\hat{\mu}})^\dagger, \quad (6)$$

where $\hat{\mu}$ is the unit vector in direction μ and \dagger denotes the hermitian conjugate. This transformation property ensures gauge invariance of observables. A sample lattice configuration collects all link variables on the lattice

$$S = (\{U_\mu^x | x \in N_\tau \times N_s \times N_s \times N_s, \mu \in \{\tau, x, y, z\}\}) . \quad (7)$$

From equation (6), it can be shown that closed loops over link variables are gauge invariant objects. The action we use in our simulations is the lattice version of the Yang-Mills action

$$S_{\text{Wilson}}[U] = \beta_{\text{latt}} \sum_x \sum_{\mu < \nu} \text{Re} \text{tr} (\mathbb{1} - U_{\mu\nu}^x), \quad (8)$$

where β_{latt} is the lattice coupling. Here $U_{\mu\nu}^x = U_\mu^x U_\nu^{x+\hat{\mu}} U_{-\mu}^{x+\hat{\mu}+\hat{\nu}} U_{-\nu}^{x+\hat{\nu}}$ is the smallest possible closed rectangular loop. The order parameter for the deconfinement phase transition is the expectation value of the Polyakov loop. The Polyakov loop

$$\begin{aligned} L(\vec{x}) &= \text{tr} \left(\prod_{x_0=0}^{N_\tau-1} U_\tau^x \right)^{N_s=2} \text{tr} (U_\tau^{0,\vec{x}} U_\tau^{1,\vec{x}}) \\ &= 2 (a_\tau^{0,\vec{x}} a_\tau^{1,\vec{x}} - b_\tau^{0,\vec{x}} b_\tau^{1,\vec{x}} - c_\tau^{0,\vec{x}} c_\tau^{1,\vec{x}} - d_\tau^{0,\vec{x}} d_\tau^{1,\vec{x}}), \end{aligned} \quad (9)$$

is another gauge invariant quantity. It is the trace of a closed loop that winds around time direction using periodic boundary conditions. The expectation value of the Polyakov loop is zero in the confined phase and finite in the deconfined phase. Another way to look at confinement is center symmetry. In the confined phase, SU(2) lattice gauge theory is symmetric under so-called center symmetry transformations. They are given by a multiplication of all temporal links at a given time slice by $z \in \{-1, 1\}$. Under those transformations, the Polyakov loop transforms as $L \rightarrow zL$. This provides a strong analogy to the Ising model, since one can view individual Polyakov loops as spins corresponding to either value of z . In the deconfined phase, this symmetry is broken and Polyakov loops favor one of the values of z .

More details on the simulations can be found in Appendix A.

III. MACHINE LEARNING PIPELINE

A. Artificial Neural Networks

In this work we employ feed-forward artificial neural networks as a tool to distinguish between two classes in the context of supervised learning. Supervised learning is the field in machine learning where the algorithm learns to classify labeled training data. After being successfully trained, the algorithm is able to predict the label of unseen test samples with high accuracy. A feed-

forward artificial neural network is a directed weighted graph consisting of layers, where only connections between neurons of neighboring layers are allowed. It has been shown that such an artificial neural network, with sufficiently many parameters, can approximate any continuous function [43, 44]. We consider a neural network as an approximation of the decision function D . The decision function assigns to each sample S a probability $P \in [0, 1]$ to be in class 1. The decision boundary is a hyperplane in the space of the parameters of sample configurations defined by $D(S) = 0.5$, where the neural network is most unsure about the correct label. If there exists an explicit quantity $Q(S)$ which is learned by the neural network, and which is responsible for the distinction between phases, we expect that a change in the quantity Q is always related to a change in the prediction probability. Hence $\nabla Q \parallel \nabla D$ in the vicinity of the decision boundary. In our neural networks the output can be written as $D(S) = \text{sigmoid}(\xi(S))$, where $\text{sigmoid}(x) = 1/(1 + \exp(-x))$ maps the latent prediction $\xi(S)$ to a probability. It follows that $\nabla Q \parallel \nabla \xi$ and thus Q can be expressed as a linear function of ξ in a linearized regime close to the decision boundary $\xi(S) = wQ(S) + b$. In the following sections we determine the latent prediction ξ and hence the decision function D as a simple function of S . Eventually, this allows us to explicitly formulate the quantity Q on which the neural network bases its classification.

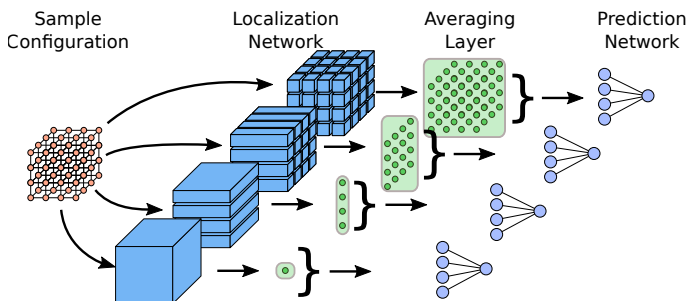


Figure 1: The **Correlation Probing Neural Network** consists of three types of neural networks stacked on top of each other. The localization network is a fully convolutional neural network which prohibits connections outside of the receptive field of each output neuron. The averaging layer averages over the input from the localization network, similarly to how the magnetization averages over all spins. The prediction network is a fully connected neural network, which transforms the output of the averaging layer to a prediction probability.

B. Ising Model

Typically, order parameters are used to distinguish between phases. They are zero in one phase and finite in the other. For example in the Ising Model, see section II A, the order parameter is the expectation value

of the magnetization $M(S) = |1/N \sum_i s_i|$. Physical order parameters obey a lot of symmetries, thus they can be formulated in closed equations with few parameters.

When machine learning algorithms and especially neural networks classify phases, they encode their decision function in a highly elusive and highly non-linear way. We pose the question if the decision function of a neural network can be expressed as a simple function of only a few specific spin correlations. In order to answer this question, we present a new type of neural network that is tailored to probe if specific correlations between spin variables contribute to the decision function of the neural network. We call it *correlation probing neural network*, see Fig. 1. The neural network architecture can be found in Appendix B. It consists of three separate subnetworks: the localization network is a fully convolutional neural network which only allows connections between sites that have a predefined relative location to each other. In other words, this network consists of identical subnetworks acting only on patches of the input sample. The receptive field size of the output neurons of the localization network is the size of each of the patches. The output of the localization layer is averaged in the averaging layer, where all information about the spatial location is lost. The prediction network is a fully connected neural network which transforms the output of the averaging layer to a prediction. If, for example, the receptive field of a neuron of the localization layer has the dimensions 1×1 , the correlation probing network can only approximate functions containing the correlation of a single spin variable with itself, as it is the case for the magnetization.

We apply the correlation probing neural network to the Ising Model by training it on Monte Carlo-sampled configurations below $T=1.6$ in the ordered phase and above $T=2.9$ in the unordered phase. More information about Monte Carlo simulation can be found in Appendix A. The training objective is to correctly predict the phase of each sample configuration, which is achieved by minimizing the binary cross entropy loss function (B1) between the correct label and the prediction. We compare the performance of the correlation probing neural network for different receptive field sizes in the localization network in Table I. Using the full receptive field of 28×28 , we allow the neural network to learn all possible spin correlations to approximate its decision function. In this case, the correlation probing network is equivalent to a standard convolutional neural network. The training and validation losses are minimized to a value close to zero. We conclude that the neural network has found all necessary information it needs to reliably classify the phases. By successively lowering the receptive field size, see Fig. 2f, we do not observe a drop in performance, except from 1×2 to 1×1 and from 1×1 to the baseline classifier, see Table I. In each of these steps the neural network loses important information about the samples which it needs to reliably classify them. In Fig. 2e we can see the average classification probability, as a function of the temperature, of both networks. This plot, the training

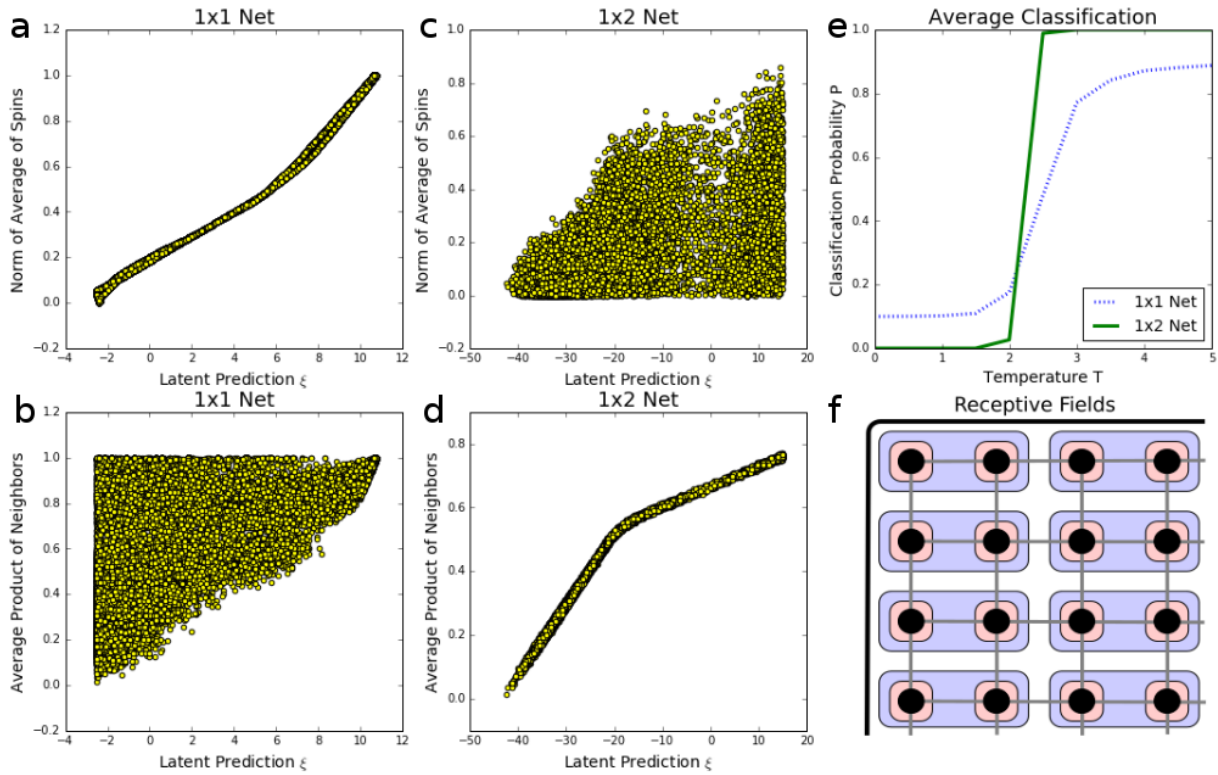


Figure 2: Results of the correlation probing neural network applied to the Ising Model. The latent prediction ξ is the argument of the sigmoid function, which is the activation function in the last layer of the prediction network. **a, b, c, d**: We calculated the values of either axis for all sample configurations and plotted them in scatterplots. **a**: The latent prediction is perfectly correlated with the absolute value of the average of spins, i.e the magnetization in the 1×1 network. **b**: It is not correlated with the average product of neighboring spins, i.e. the expected energy per site. **d**: The latent prediction of the 1×2 network is perfectly correlated with the average product of neighbors, but not with **c**: the norm of the average of spins. **e**: Average classification probability as a function of temperature. **f**: Receptive fields 1×1 , 1×2 and 28×28 of the localization network output neurons, as probed in Table I.

loss and the validation loss show that the 1×1 network is less accurate than the 1×2 network. The phase transition temperature can be found where $P = 0.5$. This is at $T = 2.5 \pm 0.5$ for the 1×1 Network and $T = 2.25 \pm 0.25$ for the 1×2 Network. An accurate estimation can be found in [16]. We however focus on examining what information got lost while lowering the receptive field size.

By construction, the decision function D of the 1×1 neural network can be expressed as

$$D(S) = F\left(\frac{1}{N} \sum_i f(s_i)\right) = \text{sigmoid}\left(\xi\left(\frac{1}{N} \sum_i f(s_i)\right)\right), \quad (10)$$

where F is the function approximated by the prediction network and f is the function approximated by the localization network. The argument of f is only a single

spin. The function f can be Taylor-expanded:

$$f(s_i) = f_0 + f_1 s_i + f_2 \underbrace{s_i^2}_1 + f_3 \underbrace{s_i^3}_{s_i} + \dots \quad (11)$$

Since $s_i^2 = 1$, all higher order terms can be neglected. The constants f_0 and f_1 can be absorbed by the bias and the weights of the prediction network approximating F . Thus, the decision function reduces to

$$D(S) = F\left(\frac{1}{N} \sum_i s_i\right). \quad (12)$$

At this point we are almost done, since all F does, is to formulate a probability $p \in [0, 1]$ from its argument. In order to determine the function F , we need to compare the latent prediction ξ of the neural network, with the argument of F : $1/N \sum_i s_i$, in the vicinity of the decision boundary. By looking at Fig. 2a, we infer that the latent prediction is given by $\xi(S) \approx w|1/N \sum_i s_i| + b$. This knowledge allows us to construct the function $F(x) \approx$

sigmoid($w|x|+b$) and thereby the decision function

$$D(S) \approx \text{sigmoid}\left(w \left| \frac{1}{N} \sum_i s_i \right| + b\right), \quad (13)$$

with weight w and bias b of the prediction neuron. The secondary purpose of this plot is to show the perfect correlation between the latent prediction $\xi(S)$ and $|1/N \sum_i s_i|$, which proves that our above deduction led to the correct result.

Until this point we have not used any information about the Ising model except Monte Carlo configurations. We have found that the decision function determines the phase by the quantity $Q(S) = |1/N \sum_i s_i|$. This function is the magnetization.

By examining the 1×2 , we require by construction that the decision function is of the form

$$D(S) = F\left(\frac{1}{N} \sum_{\langle i,j \rangle_T} f(s_i, s_j)\right). \quad (14)$$

Here the sum only goes over transversal nearest neighbors, collecting each spin only once. The Taylor expansion,

$$f(s_i, s_j) = f_{0,0} + f_{1,0} s_i + f_{0,1} s_j + f_{2,0} s_i^2 + f_{1,1} s_i s_j + f_{0,2} s_j^2 + \dots, \quad (15)$$

contains only three terms of note, all other terms can be reduced to simpler ones by using $s_i^2 = 1$. The terms $f_{1,0} s_i$ and $f_{0,1} s_j$ represent the magnetization. From Table I and the analysis of the 1×1 network, we know that these terms contain less information than the quantity we are looking for. So the leading term must be $f_{1,1} s_i s_j$. Thus, the decision function can be written as

$$D(S) \approx F\left(\frac{1}{N} \sum_{\langle i,j \rangle_T} s_i s_j\right). \quad (16)$$

In Fig. 2d we see the perfect correlation between the latent prediction $\xi(S)$ and $1/N \sum_{\langle i,j \rangle_T} s_i s_j$. This also means that the correction from the subleading terms $f_{1,0} s_i$ and $f_{0,1} s_j$ is indeed negligible. Hence we end up with the decision function

$$D(S) \approx \text{sigmoid}\left(w \left(\frac{1}{N} \sum_{\langle i,j \rangle_T} s_i s_j\right) + b\right). \quad (17)$$

By translational and rotational symmetry, the sum can be generalized to all neighbors $Q(S) = \frac{1}{N} \sum_{\langle i,j \rangle_{nn}} s_i s_j$. This quantity is, up to a minus sign, the expected energy per spin site. It is worth noting that the energy per site can be used to distinguish between phases more reliably than the magnetization, see Table I.

By examining the correlation probing neural network, we found which spatial correlations are crucial in deciding the phase. Furthermore, using this information, we reduced the complexity of the decision function so that we

were able to fully reconstruct it. From the decision function one can read out the quantity by which the neural network makes its decision about phases. The quantities we found agree with the magnetization and the average energy per spin site. Both quantities are known to have diverging derivatives with respect to the temperature, and thus are defining quantities of a phase transition either in Landau-Ginzburg-theory or Ehrenfest classification.

Receptive Field Size	Train Loss	Validation Loss
28×28	$6.1588e-04$	0.0232
1×2	$1.2559e-04$	$1.2105e-07$
1×1	0.2015	0.1886
baseline	0.6931	0.6931

Table I: Ising model: Losses of neural networks with different receptive fields of the neurons in the localization network. This is a measure of how well a neural network performs, less is better. The baseline classifier is a random classifier which predicts each phase with a probability of $p = 0.5$.

C. SU(2) Lattice Gauge Theory

We demonstrate the power of our new method at SU(2) lattice gauge theory in order to examine the deconfinement phase transition. We construct a whole machine learning pipeline around the correlation probing network, consisting of three different machine learning techniques: principal component analysis, neural networks and regression. Starting from no knowledge of an existing phase transition, we first employ unsupervised learning to get first indications about the existence and position of phases. Afterwards we train the correlation probing network to correctly predict phases. We then split the spin configurations to local configurations according to the spatial structure obtained from the correlation probing network. On these new samples, we train a local neural network to correctly classify phases. At last, we employ a regression algorithm to the local neural network results to find an explicit expression of the decision function of correlation probing neural network.

1. Unsupervised Learning of Phase Transitions

We assume no prior knowledge of the phase transition, even its existence. Hence, we employ unsupervised learning to find any possible indications for a phase transition. For the sake of simplicity we employ principal component analysis (PCA) [22, 45] with two principal components.

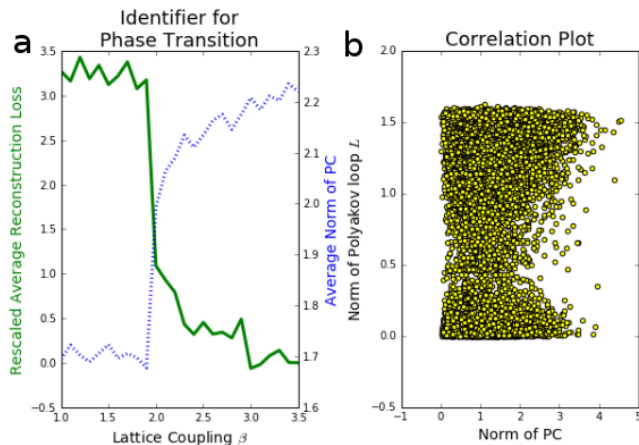


Figure 3: **a**: Finding a possible phase transition with PCA. The average mean squared error reconstruction loss as a function of temperature is a universal identifier for a phase transition. It was calculated in 100 independent PCA runs with two principal components (PC), measured in units of $\times 10^{-5}$ and shifted by the value at $\beta = 3.5$. The average norm of the PC also indicates a phase transition. **b**: There is no correlation between the principal components and the Polyakov loop.

PCA is an orthogonal linear transformation of the input samples to a set of variables, sorted by their variance. Here, unsupervised learning algorithms that are based on the reconstruction loss like autoencoders [23] are doomed to fail, since the states are gauge invariant. The autoencoder would need to predict a matrix which is not unique.

Even though the Polyakov loop is a non-linear order parameter, PCA captures indications of a phase transition at $\beta \in [1.8, 2.2]$, which is demonstrated in Fig. 3a. Here we employed the average reconstruction loss [23] and the Euclidean norm of the principal components as identifiers for a phase transition. In Fig. 3b we show that there is no correlation between the Polyakov loop and the principal components.

It is worth noting that this example shows that PCA can capture phase indicators even when the principal components cannot approximate any order parameter.

2. Correlation Probing Neural Network

We train the correlation probing neural networks with different receptive fields, see Fig. 1 and Appendix B, to predict phases on Monte Carlo-sampled configurations at lattice coupling $\beta \in [1, 1.2]$ in one phase and $\beta \in [3.3, 3.5]$ in the other phase. We test the neural network in $\beta \in [1.3, 3.2]$ to predict a phase transition at $\beta = 1.99 \pm 0.10$ ($2 \times 1 \times 1 \times 1$ network) and $\beta = 1.97 \pm 0.10$ ($2 \times 8 \times 8 \times 8$ network), see Fig. 4c. A direct calculation from the lattice configurations reveals $\beta = 1.880 \pm 0.025$, we comment on the difference in Appendix A. By successively lowering the receptive field size we lose important

Receptive Field Size	Train Loss	Validation Loss
$2 \times 8 \times 8 \times 8$	$1.0004e-04$	$2.6266e-04$
$2 \times 8 \times 1 \times 1$	$8.8104e-08$	$1.3486e-07$
$2 \times 1 \times 1 \times 1$	$7.7671e-05$	$2.0394e-04$
$2 \times 1 \times 1 \times 1$	$8.8104e-08$	$6.8276e-08$
$2 \times 1 \times 1 \times 1$ no hidden layers in prediction net	$2.2292e-07$	$4.2958e-07$
$1 \times 1 \times 1 \times 1$	0.6620	0.9482
baseline	0.6931	0.6931

Table II: SU(2): Losses of neural networks with different receptive fields of the neurons in the localization network.

information for classifying phases below $2 \times 1 \times 1 \times 1$, see Table II. This means that crucial information about the phase transition is contained in this specific structure.

The decision function of the $2 \times 1 \times 1 \times 1$ network is constrained to

$$D(S) = F\left(\frac{2}{N} \sum_{\vec{x}} f(U_{\tau}^{0,\vec{x}}, U_x^{0,\vec{x}}, U_y^{0,\vec{x}}, U_z^{0,\vec{x}}, U_{\tau}^{1,\vec{x}}, U_x^{1,\vec{x}}, U_y^{1,\vec{x}}, U_z^{1,\vec{x}})\right), \quad (18)$$

where F is a function of a single variable and f is a function of 32 variables, since each U_{μ}^x is uniquely defined by four real numbers. In order to determine the decision function, one could perform a combined polynomial fit of F and f on the latent prediction ξ . Since a feasible approach requires some knowledge about neural network architecture, we present this procedure in Appendix C.

Here we present a different approach. It is based on reducing the expressibility of the neural network even further and separating the lattice to $2 \times 1 \times 1 \times 1$ patches. First, we convince ourselves that we do not need any hidden layers in the prediction network, i.e. we only keep the output neuron, see Table V. Then the decision function simplifies to $D(S) = \text{sigmoid}(w Q(S) + b)$, where

$$Q(S) = \frac{2}{N} \sum_{\vec{x}} f(U_{\tau}^{0,\vec{x}}, U_x^{0,\vec{x}}, U_y^{0,\vec{x}}, U_z^{0,\vec{x}}, U_{\tau}^{1,\vec{x}}, U_x^{1,\vec{x}}, U_y^{1,\vec{x}}, U_z^{1,\vec{x}}) \quad (19)$$

reduces to a sum of functions acting only on a single patch of size $2 \times 1 \times 1 \times 1$ each. This allows us to split all samples to a minimum size of $2 \times 1 \times 1 \times 1$. By doing this, we enlarge the number of training samples by a factor of 512, which can enormously boost the accuracy in the following steps.

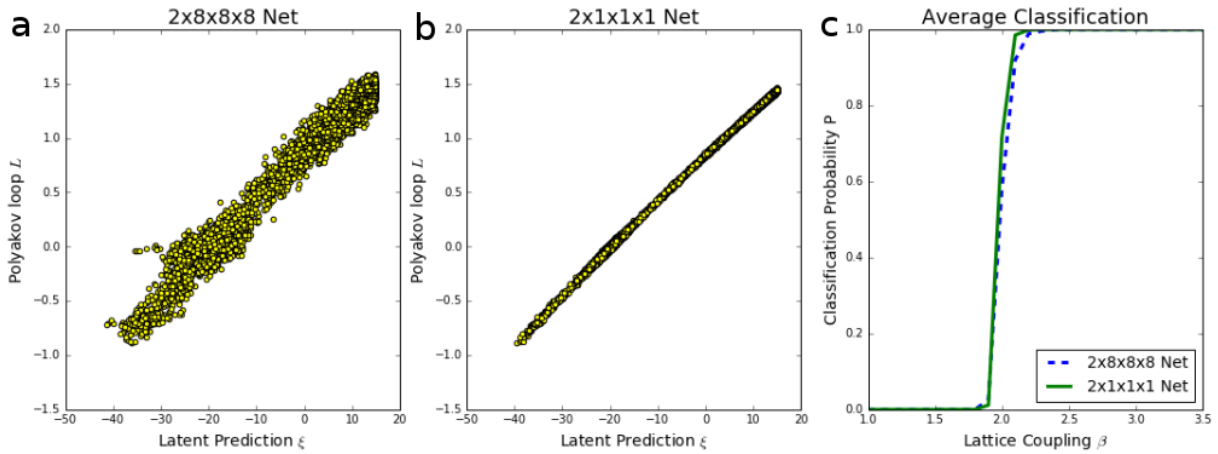


Figure 4: Results of the correlation probing network applied to SU(2) lattice gauge theory. **a,b**: The latent prediction shows a strong correlation with the Polyakov loop in both the $2 \times 8 \times 8 \times 8$ network and the $2 \times 1 \times 1 \times 1$ network. **c**: The average prediction probability of the two networks.

3. Local Neural Network Regression

We train a new neural network on the local data samples to classify the phases of each local sample. Although there is a lot more margin for error, the local neural network can now associate a prediction to each patch.

We perform a polynomial regression on the latent prediction of the local neural network on only 1% of the dataset and use another 1% as validation set. We compare different orders of regression and find that a second order polynomial performs best, see Table III. The regression approximates the latent prediction by a sum of 561 terms. We extract the weights of the regression and find that the parameter which quantifies the phase transition is given by

$$\begin{aligned}
 f(\{U_\mu^{x_0}\}) &= f(U_\tau^0, U_x^0, U_y^0, U_z^0, U_\tau^1, U_x^1, U_y^1, U_z^1) \\
 &= f((a_\tau^0, b_\tau^0, \dots, d_z^1)) \\
 &\approx +7.3816 a_\tau^0 a_\tau^1 + 0.2529 a_\tau^1 b_\tau^1 \\
 &\quad + \dots \\
 &\quad - 0.2869 d_\tau^0 c_\tau^1 - 7.2279 b_\tau^0 b_\tau^1 \\
 &\quad - 7.3005 c_\tau^0 c_\tau^1 - 7.4642 d_\tau^0 d_\tau^1. \quad (20)
 \end{aligned}$$

We only keep the leading contributions and assume that the differences between the leading contributions originate from approximation errors. In this way we can justify errors of the size of the next to leading coefficients. Since overall factors and intercepts can be absorbed in the weights and biases of the neural network, we can simply rescale the above parameter to

$$\begin{aligned}
 f((a_\tau^0, b_\tau^0, \dots, d_z^1)) &\approx a_\tau^0 a_\tau^1 - b_\tau^0 b_\tau^1 - c_\tau^0 c_\tau^1 - d_\tau^0 d_\tau^1 \\
 &= \text{tr}(U_\tau^0 U_\tau^1). \quad (21)
 \end{aligned}$$

This is the Polyakov loop on a single spatial lattice site

(9). We promote $f(\{U_\mu^{x_0}\}) \rightarrow f(\{U_\mu^{x_0, \vec{x}}\})$ to act on the full lattice, such that we can formulate the decision function of the neural network with the full receptive field as

$$D(S) \approx \text{sigmoid} \left(w \left(\frac{2}{N} \sum_{\vec{x}} f(\{U_\mu^{x_0, \vec{x}}\}) \right) + b \right). \quad (22)$$

Here $Q(S) = \frac{2}{N} \sum_{\vec{x}} f(\{U_\mu^{x_0, \vec{x}}\})$ is the Polyakov loop on the full lattice. A confirmation of this deduction can be seen in the perfect correlation between the latent prediction and the Polyakov loop in Fig. 4a,b.

Order of Regression	Train Score	Validation Score
Polynomial Regression		
1	0.00128	-0.00042
2	0.72025	0.72395
3	0.75675	0.69129
Support Vector Regression		
1	-0.08943	-0.08988
2	0.64048	0.65367
3	-0.08434	-0.08963

Table III: Scores of different regression algorithms. Higher is better.

IV. CONCLUSION

We have combined the analyses of previous works and presented a pipeline of several machine learning algorithms which find the existence of different phases and predict the position of the phase transition. The most

important result of our work is the explicit calculation of the decision functions of the neural networks classifying the phases of the Ising model, see equations (13) and (17), and the decision function of the neural network applied to SU(2) lattice gauge theory, see equation (22).

For this purpose, we proposed the correlation probing neural network. By employing this network we analyzed the complexity and the symmetries of the decision function. The results of the correlation probing network enabled us to reconstruct the decision function in a simple form and thereby reveal the explicit formula of the quantity by which the neural network distinguishes between phases. The method was introduced at the Ising model on the square lattice, where the decision functions contain the formulas of the magnetization or of the expected energy per site. We then demonstrated the power of this new method at SU(2) lattice gauge theory, where the reconstructed decision function reveals the explicit mathematical expression of the Polyakov loop, a non-linear, non-local order parameter.

As of now machine learning is able to construct formulas of physical quantities relevant to phase transitions. This could find application in strongly correlated systems where the nature of the phases is unknown. Such systems include QCD at high densities and the two dimensional Hubbard model at finite chemical potential.

We hope to see further developments based on our approach: (i) It would be interesting to see how to extract order parameters when it is not possible to find a reduction to a semi local order parameter. This could be the case for example in the incommensurate antiferromagnetic phase in high-temperature superconductors. (ii) Machine learning performs better if it is trained on appropriate features. Our approach could also be used to decide on what features to generate from raw data, similar to, or as an extension to quantum loop tomography [20]. (iii) Our method of finding an order parameter can be expanded to unsupervised learning by embedding it into an autoencoder [23]. (iv) It would also be interesting to study if this new approach can give insight in what neural networks learn in other disciplines, such as computer vision.

Acknowledgments We would like to thank Jan M. Pawłowski, Manfred Salmhofer, Ion-Olimpiu Stamatescu and Christof Wetterich for useful discussions. We thank Shirin Nkongolo for reviewing the manuscript. S.W. acknowledges support by the Heidelberg Graduate School of Fundamental Physics. M.S. is supported by the DFG via project STA283/16-2.

Appendix A: Monte Carlo Simulations

In statistical physics and lattice gauge theory, Markov Chain Monte Carlo algorithms are used to sample lattice configurations from the Boltzmann factor. This is done by constructing a stochastic sequence that starts at some random initial configuration. This stochastic se-

quence is constructed such that the configurations obey Boltzmann statistics in the equilibrium. For more details on algorithm requirements and algorithms see e.g. [46].

Observables are then computed by taking the average over many spin or lattice configurations from the equilibrium distribution

$$\langle \mathcal{O} \rangle = \lim_{N \rightarrow \infty} \frac{1}{N} \sum_{i=1}^N \mathcal{O}_i . \quad (\text{A1})$$

Taking the limit in the last equality is practically not possible. Hence, the expectation value of the observable is approximated by large N and gives rise to a statistical error. It is important to take enough configurations such that ergodicity is achieved. In the case of two distinct regions of phase space, this can take very long simulation time.

For the Ising model, we produced a total of 55000 spin configurations, of size 28×28 , equally distributed over eleven equidistant temperature values $T \in [0, 5]$ by employing the Metropolis-Hastings algorithm [47] with simulated annealing.

For SU(2), we used the Heatbath algorithm [48] to produce a total of 15600 decorrelated configurations equally distributed over 26 values in the range of $\beta_{\text{latt}} = 4/g^2 \in [1, 3.5]$. In the context of this paper it is important to have decorrelated data, since neural networks are good at finding structures, and thus correlations between configurations, if existent. Due to center symmetry breaking, in the deconfined phase the average Polyakov loop can take either positive or negative values of equal magnitude, hence one usually takes the absolute value as an order parameter. At large values of β_{latt} , this will prevent a full exploration of phase space. In our simulations, we initiated all links with the unit matrix, hence we introduced a bias for large values of β_{latt} , i.e. our simulations are not fully ergodic. If we were to employ neural networks to extract the position of the phase transition, this non-ergodicity would lead to a shift in the value of critical β_{latt} . Generally speaking, ergodicity can be retained by doing more simulations and employing algorithms such as simulated annealing or overrelaxation, thus in principle it should be possible to extract the critical temperature reliably.

Appendix B: Neural Network Architecture

We constructed our machine learning pipeline using Scikit-learn [49] and Keras [50]. The neural network architectures are presented in Tables IV and V. Since there is no Convolutional4D in Keras, we just rearranged our samples to fit a Convolutional1D Layer. We used neural networks with number of filters $n_A, n_B, n_D \in \{1, 4, 8, 32, 256, 1024\}$. The kernel sizes A, B, C are used to set the receptive field size. For our problems, $n_C = 1$ is sufficient to capture the structure of the order parameter. This was probed in the same manner as finding

the optimal receptive field size. In other models one might need a higher n_C , e.g. in the Heisenberg model, $n_C = 3$ could be optimal. Hence, this can already be an early indicator for the type of the broken symmetry. The activation functions are rectified linear units $\text{relu}(x) = \max(0, x)$ between all layers and the sigmoid function $\text{sigmoid}(x) = 1/(1 + \exp(-x))$ in the last layer. We do not employ any sort of regularization. The training objective is minimizing the binary cross entropy loss function

$$C(Y, P) = -\frac{1}{N} \sum_i (y_i \log p_i + (1 - y_i) \log(1 - p_i)) , \quad (\text{B1})$$

where $Y = y_i$ is a list of labels and $P = p_i$ is the corresponding list of predictions. Our baseline classifier is the classifier which assigns each label with a probability of $p_i = 0.5$. This means that this classifier just assigns a label to each sample randomly. The binary cross entropy then evaluates to 0.6931. The neural networks learn by optimizing the weights and biases via RMSprop gradient descent. The neural networks were trained for 300 epochs or less, if the loss already saturated in earlier epochs. The validation set is 20% of the training data.

Layer	Output Shape	Kernel Size
<i>InputLayer</i>	(784, 1)	
<i>Convolution1D</i>	(784/(A), n_A)	A
<i>Convolution1D</i>	(784/(A × B), n_B)	B
<i>Convolution1D</i>	(784/(A × B × C), n_C)	C
<i>AveragePooling</i>	(1, n_C)	
<i>Flatten</i>	(n_C)	
<i>Dense</i>	(n_D)	
<i>Dense</i>	(1)	

Table IV: Ising Model Neural Network. A, B, C determine the receptive field size of each neuron in the averaging layer.

Layer	Output Shape	Kernel Size
<i>InputLayer</i>	(1024, 16)	
<i>Convolution1D</i>	(1024/(A), n_A)	A
<i>Convolution1D</i>	(1024/(A × B), n_B)	B
<i>Convolution1D</i>	(1024/(A × B × C), n_C)	C
<i>AveragePooling</i>	(1, n_C)	
<i>Flatten</i>	(n_C)	
<i>Dense</i>	(n_D)	
<i>Dense</i>	(1)	

Table V: SU(2) Neural Network. A, B, C determine the receptive field size of each neuron in the averaging layer.

Appendix C: Regression of the Polyakov Loop

The decision function of the $2 \times 1 \times 1 \times 1$ neural network which predicts the lattice SU(2) phase transition is by construction

$$D(S) = F \left(\frac{2}{N} \sum_{\vec{x}} f(U_{\tau}^{0, \vec{x}}, U_x^{0, \vec{x}}, U_y^{0, \vec{x}}, U_z^{0, \vec{x}}, U_{\tau}^{1, \vec{x}}, U_x^{1, \vec{x}}, U_y^{1, \vec{x}}, U_z^{1, \vec{x}}) \right) . \quad (\text{C1})$$

In general, we cannot assume that the prediction network consists only of the output neuron. Therefore, we suggest a different procedure for constructing the decision function. We split the full correlation probing net into subnetworks: we extract the localization network plus averaging layer and the prediction network as separate networks. In order to determine $F(S) = \text{sigmoid}(\xi(S))$, we use polynomial regression to fit the latent prediction of the prediction network to the output of the averaging layer. We find a polynomial of degree 1 is enough to fit the data, and ξ is approximated by

$$\xi(x) \approx -0.7101 x + 9.85143419 . \quad (\text{C2})$$

The slope and intercept can be absorbed by the weight w and bias b of the output neuron, such that we can infer

$$\xi(x) \approx w x + b . \quad (\text{C3})$$

The function f requires us to build a new local neural network which only acts on patches of size $2 \times 1 \times 1 \times 1$. By construction this network has the same number of weights and biases, as the full neural network acting on the input of size $2 \times 8 \times 8 \times 8$. Instead of training the local neural network, we transfer the the weights and biases from the full correlation probing network to the local neural network. Hence, one can obtain the output of the localization network for each patch separately. Again, we employ polynomial regression to fit the input from the local patches to the output of the localization network. The result of a regression of degree 2 with 561 parameters yields

$$\begin{aligned} f(\{U_{\mu}^{x_0}\}) &= f(U_{\tau}^0, U_x^0, U_y^0, U_z^0, U_{\tau}^1, U_x^1, U_y^1, U_z^1) \\ &= f((a_{\tau}^0, b_{\tau}^0, \dots, d_z^1)) \\ &\approx -26.8354 a_{\tau}^0 a_{\tau}^1 - 2.4972 d_{\tau}^0 c_{\tau}^1 \\ &\quad + \dots \\ &\quad + 1.5653 b_{\tau}^0 c_{\tau}^0 + 26.5908 b_{\tau}^0 b_{\tau}^1 \\ &\quad + 27.7054 c_{\tau}^0 c_{\tau}^1 + 27.8939 d_{\tau}^0 d_{\tau}^1 . \end{aligned} \quad (\text{C4})$$

After absorbing overall factors and the intercept by the weights and biases of the prediction network and neglecting the subleading terms, we rewrite f as

$$f((a_{\tau}^0, b_{\tau}^0, \dots, d_z^1)) \approx a_{\tau}^0 a_{\tau}^1 - b_{\tau}^0 b_{\tau}^1 - c_{\tau}^0 c_{\tau}^1 - d_{\tau}^0 d_{\tau}^1 . \quad (\text{C5})$$

This is the Polyakov loop on a single lattice site (9). By employing (C5) as an argument of (C3), we can promote $f(\{U_\mu^{x_0}\}) \rightarrow f(\{U_\mu^{x_0, \vec{x}}\})$ to depend on space again. We obtain the definition of the decision function

$$D(S) \approx \text{sigmoid} \left(w \left(\frac{2}{N} \sum_{\vec{x}} f(\{U_\mu^{x_0, \vec{x}}\}) \right) + b \right), \quad (\text{C6})$$

where $Q(S) = \left(\frac{2}{N} \sum_{\vec{x}} f(\{U_\mu^{x_0, \vec{x}}\}) \right)$ is the Polyakov loop on the full lattice.

-
- [1] Alex Krizhevsky, Ilya Sutskever, and Geoffrey E Hinton. Imagenet classification with deep convolutional neural networks. In *Advances in neural information processing systems*, pages 1097–1105, 2012.
- [2] Geoffrey Hinton et al. Deep neural networks for acoustic modeling in speech recognition: The shared views of four research groups. *IEEE Signal Processing Magazine*, 29(6):82–97, nov 2012. doi:10.1109/msp.2012.2205597.
- [3] David Silver et al. Mastering the game of go with deep neural networks and tree search. *Nature*, 529(7587):484–489, jan 2016. doi:10.1038/nature16961.
- [4] G. Carleo and M. Troyer. Solving the quantum many-body problem with artificial neural networks. *Science*, February 2017.
- [5] Giacomo Torlai and Roger G. Melko. Learning thermodynamics with boltzmann machines. *Physical Review B*, 94(16), oct 2016. doi:10.1103/physrevb.94.165134.
- [6] D.-L. Deng, X. Li, and S. Das Sarma. Exact machine learning topological states. *ArXiv e-prints*, September 2016.
- [7] D. Crawford, A. Levit, N. Ghadermarzy, J. S. Oberoi, and P. Ronagh. Reinforcement learning using quantum boltzmann machines. *ArXiv e-prints*, December 2016.
- [8] D.-L. Deng, X. Li, and S. Das Sarma. Quantum entanglement in neural network states. *ArXiv e-prints*, January 2017.
- [9] X. Gao and L.-M. Duan. Efficient representation of quantum many-body states with deep neural networks. *ArXiv e-prints*, January 2017.
- [10] G. Torlai, G. Mazzola, J. Carrasquilla, M. Troyer, R. Melko, and G. Carleo. Many-body quantum state tomography with neural networks. *ArXiv e-prints*, March 2017.
- [11] Ken-Ichi Aoki and Tamao Kobayashi. Restricted boltzmann machines for the long range ising models. *Modern Physics Letters B*, 30(34):1650401, dec 2016. doi:10.1142/s0217984916504017.
- [12] G. Kasieczka, T. Plehn, M. Russell, and T. Schell. Deep-learning top taggers or the end of qcd? *ArXiv e-prints*, January 2017.
- [13] Li Huang and Lei Wang. Accelerated monte carlo simulations with restricted boltzmann machines. *Physical Review B*, 95(3), jan 2017. doi:10.1103/physrevb.95.035105.
- [14] Junwei Liu, Yang Qi, Zi Yang Meng, and Liang Fu. Self-learning monte carlo method. *Physical Review B*, 95(4), jan 2017. doi:10.1103/physrevb.95.041101.
- [15] N. Portman and I. Tamblin. Sampling algorithms for validation of supervised learning models for ising-like systems. *ArXiv e-prints*, November 2016.
- [16] Juan Carrasquilla and Roger G. Melko. Machine learning phases of matter. *Nature Physics*, feb 2017. doi:10.1038/nphys4035.
- [17] P. Broecker, J. Carrasquilla, R. G. Melko, and S. Trebst. Machine learning quantum phases of matter beyond the fermion sign problem. *ArXiv e-prints*, August 2016.
- [18] Li Li, Thomas E. Baker, Steven R. White, and Kieron Burke. Pure density functional for strong correlation and the thermodynamic limit from machine learning. *Physical Review B*, 94(24), dec 2016. doi:10.1103/physrevb.94.245129.
- [19] K. Ch’ng, J. Carrasquilla, R. G. Melko, and E. Khatami. Machine learning phases of strongly correlated fermions. *ArXiv e-prints*, September 2016.
- [20] Y. Zhang and E.-A. Kim. Quantum loop topography for machine learning. *ArXiv e-prints*, November 2016.
- [21] F. Schindler, N. Regnault, and T. Neupert. Probing many-body localization with neural networks. *ArXiv e-prints*, April 2017.
- [22] Lei Wang. Discovering phase transitions with unsupervised learning. *Physical Review B*, 94(19), nov 2016. doi:10.1103/PhysRevB.94.195105.
- [23] S. J. Wetzel. Unsupervised learning of phase transitions: from principal component analysis to variational autoencoders. *ArXiv e-prints*, March 2017.
- [24] Evert P. L. van Nieuwenburg, Ye-Hua Liu, and Sebastian D. Huber. Learning phase transitions by confusion. *Nature Physics*, feb 2017. doi:10.1038/nphys4037.
- [25] W. Hu, R. R. P. Singh, and R. T. Scalettar. Discovering phases, phase transitions and crossovers through unsupervised machine learning: A critical examination. *ArXiv e-prints*, March 2017.
- [26] P. Ponte and R. G. Melko. Kernel methods for interpretable machine learning of order parameters. *ArXiv e-prints*, April 2017.
- [27] Geoffrey Towell and Jude W. Shavlik. Interpretation of artificial neural networks: Mapping knowledge-based neural networks into rules. In J. E. Moody, S. J. Hanson, and R. P. Lippmann, editors, *Advances in Neural Information Processing Systems 4*, pages 977–984. Morgan-Kaufmann, 1992.
- [28] A. Mahendran and A. Vedaldi. Understanding deep image representations by inverting them. *ArXiv e-prints*, November 2014.
- [29] Zoubin Ghahramani. Probabilistic machine learning and artificial intelligence. *Nature*, 521(7553):452–459, may 2015. doi:10.1038/nature14541.
- [30] R. Shwartz-Ziv and N. Tishby. Opening the black box of deep neural networks via information. *ArXiv e-prints*, March 2017.
- [31] Mark G. Alford, Andreas Schmitt, Krishna Rajagopal, and Thomas Schäfer. Color superconductivity in dense quark matter. *Reviews of Modern Physics*, 80(4):1455–

- 1515, nov 2008. doi:10.1103/revmodphys.80.1455.
- [32] M. A. Stephanov. QCD PHASE DIAGRAM AND THE CRITICAL POINT. *International Journal of Modern Physics A*, 20(19):4387–4392, jul 2005. doi:10.1142/s0217751x05027965.
- [33] J. B. Kogut and M. A. Stephanov. The phases of quantum chromodynamics: From confinement to extreme environments. *Camb. Monogr. Part. Phys. Nucl. Phys. Cosmol.*, 21:1–364, 2004.
- [34] C. M. Varma. Theory of the pseudogap state of the cuprates. *Physical Review B*, 73(15), apr 2006. doi:10.1103/physrevb.73.155113.
- [35] Louis Taillefer. Scattering and pairing in cuprate superconductors. *Annual Review of Condensed Matter Physics*, 1(1):51–70, aug 2010. doi:10.1146/annurev-conmatphys-070909-104117.
- [36] Yayu Wang, N. P. Ong, Z. A. Xu, T. Kakeshita, S. Uchida, D. A. Bonn, R. Liang, and W. N. Hardy. High field phase diagram of cuprates derived from the nernst effect. *Physical Review Letters*, 88(25), jun 2002. doi:10.1103/physrevlett.88.257003.
- [37] S Hübner, M A Hossain, A Damascelli, and G A Sawatzky. Two gaps make a high-temperature superconductor? *Reports on Progress in Physics*, 71(6):062501, may 2008. doi:10.1088/0034-4885/71/6/062501.
- [38] S. Friederich, H. C. Krahl, and C. Wetterich. Functional renormalization for spontaneous symmetry breaking in the hubbard model. *Physical Review B*, 83(15), apr 2011. doi:10.1103/physrevb.83.155125.
- [39] T. A. Maier, M. Jarrell, T. C. Schulthess, P. R. C. Kent, and J. B. White. Systematic study of d-wave superconductivity in the 2d repulsive hubbard model. *Physical Review Letters*, 95(23), nov 2005. doi:10.1103/physrevlett.95.237001.
- [40] S. Raghu and S. A. Kivelson. Superconductivity from repulsive interactions in the two-dimensional electron gas. *Physical Review B*, 83(9), mar 2011. doi:10.1103/physrevb.83.094518.
- [41] Christoph J. Halboth and Walter Metzner. d-wave superconductivity and pomeranchuk instability in the two-dimensional hubbard model. *Physical Review Letters*, 85(24):5162–5165, dec 2000. doi:10.1103/physrevlett.85.5162.
- [42] Lars Onsager. Crystal statistics. i. a two-dimensional model with an order-disorder transition. *Physical Review*, 65(3-4):117–149, feb 1944. doi:10.1103/physrev.65.117.
- [43] G. Cybenko. Approximation by superpositions of a sigmoidal function. *Mathematics of Control, Signals, and Systems*, 2(4):303–314, dec 1989. doi:10.1007/bf02551274.
- [44] Kurt Hornik. Approximation capabilities of multilayer feedforward networks. *Neural Networks*, 4(2):251–257, jan 1991. doi:10.1016/0893-6080(91)90009-t.
- [45] Karl Pearson. LIII.on lines and planes of closest fit to systems of points in space. *Philosophical Magazine Series 6*, 2(11):559–572, nov 1901. doi:10.1080/14786440109462720.
- [46] Christof Gattringer and Christian B. Lang. *Quantum Chromodynamics on the Lattice*. Springer Berlin Heidelberg, 2010. doi:10.1007/978-3-642-01850-3.
- [47] Nicholas Metropolis and S. Ulam. The monte carlo method. *Journal of the American Statistical Association*, 44(247):335–341, sep 1949. doi:10.1080/01621459.1949.10483310.
- [48] Michael Creutz. Monte carlo study of quantized SU(2) gauge theory. *Physical Review D*, 21(8):2308–2315, apr 1980. doi:10.1103/physrevd.21.2308.
- [49] F. Pedregosa et al. Scikit-learn: Machine learning in Python. 12:2825–2830, 2011.
- [50] François Chollet. keras. <https://github.com/fchollet/keras>, 2015.